Duple mondnet: duple deep learning based mobile net for motor neuron disease identification

Sony HELEN[1, *], Joseph JAWHAR[2]

[1]Department of Computer Science Engineering, Anna University, Chennai, Tamil Nadu, India

[2] Department of Electrical and Electronics Engineering, Arunachala College of Engineering for Women, Manavilai, Nagercoil, Kanyakumari, India

***Correspondence:** sonyhelen20@gmail.com

Sony HELEN: https://orcid.org/0009-0003-4463-0506

Joseph JAWHAR: https://orcid.org/0009-0001-1266-0984

Acknowledgment

The authors would like to thank the reviewers for all of their careful, constructive and insightful comments in relation to this work.

Conflict of interest

The authors declare that they have no known competing financial interests or personal relationships that could have appeared to influence the work reported in this paper.

Informed consent

I certify that I have explained the nature and purpose of this study to the above-named individual, and I have discussed the potential benefits of this study participation. The questions the individual had about this study have been answered, and we will always be available to address future questions.

Duple mondnet: duple deep learning based mobile net for motor neuron disease identification

Abstract

Background/aim: A motor neuron disease is a devastating neuron ailment that affect the motor neurons which regulates muscular voluntary actions. It is a rare disorder that gradually destroys portions of the neurological function. In general, Motor Neuron Disease (MND) appears as a result of the combination of natural, behavioural, genetic influences. However, early detection of motor neuron disease is a challenging task, manual identification is time consuming.

Materials and methods: To overcome this issue a novel deep learning-based Duple feature extraction framework has been proposed for early detection of motor neuron disease. Diffusion tensor imaging tractography (DTI) images are initially analyzed for color and textural features by using dual feature extraction. Local binary pattern (LBP) - based methods extract textural data from an image by examining nearby pixel values. A Color Information Feature is then added to the LBP-based feature during the classification phase for extracting color features. A flattened image is then fed into MobileNet for classifying normal and abnormal cases of MND based on its color, texture features.

Results: As a result, proposed Deep-MONDNet is suitable because it achieves a 99.66% of detection rate and identify disease in its early stages.

Conclusion: A Mobile Net model achieves an overall f1-score of 13.26%, 6.15%, 5.56%, and 5.96% over BPNN, CNN, SVM-RFE, and MLP, respectively.

Key words: Motor neuron disease, gaussian adaptive bilateral filter, color information feature, local binary pattern, deep learning

1. Introduction

The motor neuron disease (MND) is a group of debilitating neurodegenerative diseases harming neural units that govern voluntary movements of the muscles [1,2]. These diseases, which include Amyotrophic Lateral Sclerosis (ALS), Primary Lateral Sclerosis (PLS), and Progressive Muscular Atrophy (PMA), are characterized by the gradual degeneration of motor neurons, leading to muscle weakness, atrophy, and eventually paralysis [3,4]. Early diagnosis and effective management of MND are crucial for improving the quality of life for affected individuals, but this often presents a significant challenge due to the complexity and heterogeneity of these conditions [5,6].

Deep learning has been an effective method for illness categorization and analysis of medical images over the past decade. Convolutional Neural Network (CNN) [7], and Recurrent Neural Network (RNN) in particular have demonstrated amazing ability in extracting key characteristics from clinical records, electrodiagnostic data, and clinical imagery [8]. These models aid in the early detection and accurate classification of motor neuron diseases by analysing various data sources, such as electromyography (EMG) signals, magnetic resonance imaging (MRI) scans [9], and patient clinical histories [10]. Leveraging deep learning for MND classification not only holds the potential to streamline the diagnostic process but also to identify subtle patterns and biomarkers that might otherwise go unnoticed by human clinicians [11].

One of the key advantages of deep learning [12] in motor neuron disease classification is its ability to learn from vast datasets. By training on diverse and extensive datasets containing information from patients with various disease stages and demographics, deep learning models generalize their knowledge, enhancing their diagnostic accuracy [13]. Additionally, deep learning is not limited to a single data type; it integrates information

from multiple sources, such as, genetic profiles, and clinical notes, to provide a comprehensive understanding of the disease. This multi-modal [14] approach holds promise for a more holistic assessment of motor neuron diseases [15]. The average lifespan of someone with MND is two to three years after diagnosis, though individual circumstances may change this. Many years may pass after a diagnosis for some people. The early stage of MND and it is hardly possible to diagnosis. Artificial intelligence (AI) [16] has proliferated in recent years across all scientific disciplines. The early detection of MND is now more accurate and precise thanks to the application of AI in medicine. However, early detection of MND is a challenging task and manual identification is time consuming. To overcome these challenges, a novel deep learning-based Duple-MONDNet model has been proposed for identifying the healthy and patients affected by MND. By employing advanced deep learning models such as CNN, long short term memory (LSTM), You only look once (YOLO) [17], and so on contribute to detecting MND illnesses. The key contribution of the proposed Duple-MONDNet model be as follows.

- Initially, the Diffusion tensor imaging tractography (DTI) images are put into the duple feature extraction phase for extracting the color and textural features of the images.
- The LBP-based method extracts the textural data of an image by considering the neighbouring pixel values.
- Then, CIF is added with the LBP-based feature for color feature extraction in the classification phase.
- Afterward, the extracted color and texture features of images are flattered and given as the input to Mobile Net for classifying the MND.

- Finally, the Mobile Net is employed for classifying the normal and abnormal cases of MND.

The research's last phase was organized as follows. The relevant studies are summarized in detail in Section 2, the proposed Duple-MONDNet for detecting motor neuron disorder is explained in detail in Section 3, and the experimental findings and comments are presented in Section 4. The essay is concluded in Section 5, which goes through additional research.

2. Literature Survey

In the past, numerous researchers have used digital image processing and classification techniques to publish studies recognizing both normal and abnormal cases of MND. Diverse literature works have been written about recent developments in deep learning and machine learning techniques.

In 2019 Agosta, F et al., [18] developed a significant cohort of people with MND and the prognostic effect of multimodal brain MRI on survival. Multivariable Medical and mental features were used to build the Royston-Parmar survival model. The integrated clinical and MRI model with specific front-temporal grey matter densities and mobility vector MRI parameters achieves an AUC of 0.89.

In 2019 Lauraitis, A et al., [19] suggested proposed smartphone app for automated decision aid for cognitive task-based assessment of motor diseases of the neuron system. A back-propagation neural network (BPNN) classifier is utilized for examine the data and provide result. The rate of success in identifying early, prodromal symptoms of motor illnesses is 86.4%. The proposed method shows the low reliability rate than other models.

In 2019 Hassanpour, A et al., [20] propose a multi-class motor imaging electroencephalogram signal classification end-to-end deep neural network. Deep Belief Networks (DBN) and Stacked Sparse Autoencoder (SSAE), two Generative Deep Learning (GDL) frameworks, are used in an e2e fashion. Additionally, the effectiveness of the suggested methodology is assessed both with and without the CS and NR phases. For the Deep Belief Networks (DBN) frameworks, the suggested method attained reliability are 91.54% and 90.21%, accordingly.

In 2020 Ramakrishnan, J et al., [21] designed a cross power spectral density-based wheelchair control system for the detection of motor neuron disease. The CNN model is employed for the detection of MND using the eye movement of the people. Qualified users in the evaluation achieved a total reliability of 93.51% and still the suggested method obtained the less accurate rate than other existing methods.

In 2020 Zhang, K et al., [22] designed a hybrid neural network to enhance the detection of motor imagery signals. Enhance the ability to classify motor functions, the generative adversarial network has been presented. A short-time Fourier transform (STFT) is used to convert the time sequence data into spectrogram visuals. The hybrid network deep convolutional generative adversarial network (DCGAN) fared better than previous categorization and achieve reliability with average kappa scores of 0.564 and 0.677 from dataset. The obtained accuracy level is still not enough.

In 2021 Greco, A et al., [23] suggest utilizing only blood data to identify and classify patients with participation of both higher and lesser motor neuron. For categorizing each patient into the ALS or Lower motor neuron (LMN) disease classes, a support vector machine with recursive feature elimination (SVM-RFE) was implemented. The

experiment yield 94% of accuracy rate for the classification and the outcome shows less rate than other approaches.

In 2021 Subasi, A et al., [24] suggest a powerful combination of the Multiscale Principal Component Analysis (MSPCA), and ensembles learning-based algorithms for the classification of the MND. Employing ECG signals, a wavelet transform (WT) based on the Daubechies method is used to produce the noise reduction. The stated ensemble learning method produces accuracy values of 98.69% and 94.83% respectively.

In 2022 Sekar, G et al., [25] proposed a neural machine learning model to recognize motor neuron illness and forecast its effects on health. Based on historical data and current knowledge, the machine learning system forecasts the effects of motor neuron illness. Using the above symptoms, it may be concluded that there is 93.28% bulbar palsy, 91.44% tendon erosion, and 93.22% polytopic paralysis. The experiment attains low level of reliability rate.

In 2022 Bede, P et al., [26] presented Motor neuron illness phenotypic classification of each patient using radiological disease load variations. Applying the Multilayer Perceptron (MLP) rate of classification for amyotrophic lateral sclerosis was achieved 93.7%, while poor accurate diagnosis was found for primary lateral sclerosis 43.8%. The experimental provides the low level of success rate for the classification of illness.

In 2023 Toh, C et al., [27] suggest spinal and brain MRI measurements in a single region for the direct neurodegeneration in motor neuron illness. A collection of 75 MND patients and 13 normal controls possessed MRI. Utilizing Free Surfer, volumetric T1-weighted images were used to quantify the precentral gyral width. The experiment achieves 95% of success rate, but the reliability level is not enough for the detection.

According to the studies described above, the MND has detected utilizing several kinds of techniques. To determine and categorize disease, researchers employed approaches like preliminary processing images, and categorizing diseases using some training models. The techniques utilized are provide low reliability rate than advance deep learning approaches. To overcome this a novel Duple MONDNet is proposed for the early detection of MND.

3. Proposed Method

In this research paper, a novel deep learning-based Duple-MONDNet model has been proposed for identifying the healthy and patients affected by MND. Initially, the fruit images are fed into the dual-feature extraction phase for extracting the color and textural features of the images. The LBP-based operator extracts the textural data of an image by considering the neighbouring pixel values. Then, CIF is added with the LBP-based feature for color feature extraction in the classification phase. Afterward, the extracted color and texture features of images are flattered and given as the input to Mobile Net for classifying the normal and abnormal cases. Finally, the Mobile Net is employed for classifying early stages of MND. Figure 1 depicts the proposed Duple-MONDNet.

3.1. Dataset Description

In this section, the gathered dataset and the data augmentation process are evaluated to enhance the images in the dataset and detect MND. The images are collected from Pranav Diagnostics Centre in Nagercoil, Tamil Nadu. The dataset comprises 78 normal cases and 52 abnormal images. To enhance the dataset, the collected images underwent augmentation. The study's experimental setup was conducted using Spyder, an Anaconda navigator, running on a PC equipped with Windows 10 OS. The PC featured an Intel i5 core processor with a clock speed of 2.10 GHz and a 16GB RAM system. Additionally,

the performance of the proposed model was evaluated with several other deep learning models.

Table 1 displays the distribution of disease classes in the dataset before and after augmentation. Initially, the dataset consisted of 130 total images sourced from our self-prepared dataset, with 78 representing normal brain scans and 52 representing abnormal brain scans. Following augmentation, the dataset experienced significant expansion, with the total number of images increasing to 3120 for the self-prepared dataset. Notably, the augmentation process substantially increased the number of normal images to 1872 from the self-prepared dataset, while the number of abnormal images similarly rose to 1248 from the self-prepared dataset. As a result, the augmented dataset now comprises a total of 3250 images, providing a larger and more balanced dataset for training and analysis purposes.

3.2. Gaussian adaptive bilateral (GAB) filter

The GAB filter is used at the pre-processing stage to reduce the distortion in the input images. The principle of bilateral filtering is combined with adaptive parameter adjustments in the Gaussian Adaptive Bilateral Filter, which effectively denoises medical images. It is crucial for the identification of motor illnesses by deep learning since efficient data maintaining is required for reliable diagnosis and evaluation. The method proposed significantly enhance the quality of images. The bilateral filter and input image I_p and guidance G_d are different, as shown in equation (1):

$$f(v) = \sum_u \left(W_{v,u}^{G_d} \right) (G_d) I_u \quad (1)$$

Where I_u represent the source image and $W_{v,u}^{G_d}$ is demonstrated in below equation (2).

$$W_{v,u}^{G_d} = \frac{1}{Nor_f} \exp\left[- \left\| \frac{v-u}{-\sigma_z^2} \right\|^2 \right] \quad (2)$$

From the above equation (2) Nor_f denotes the normalizing factor. In equation (2) Gaussian spatial filter is depicted by $\exp\left[-\left\|\frac{v-u}{-\sigma_z^2}\right\|^2\right]$, the GAB kernel is expressed in equation (3).

$$\mathfrak{H}_{v,u}^{gab}(I, G^-) = \frac{1}{Nor_f}\exp\left[-\left\|\frac{v-u}{-\sigma_z^2}\right\|^2\right] exp\left[-\left\|\frac{I_v - G_d{}^-}{-\sigma_s^2}\right\|^2\right] \quad (3)$$

Where, $-\sigma_z^2$ represent the difference in intensities. $G_d{}^-$ obtained from equations (1) and (3) and $exp\left[-\left\|\frac{I_v - G_d{}^-}{-\sigma_s^2}\right\|^2\right]$ is the range kernel.

$$f(v) = \sum_v \left(W_{v,u}^{gab_f}\right)[I_p, G_d{}^-]I_u \quad (4)$$

The final output $f(v)$ of the GAB filter is expressed in equation (4). The noise-free images are used as input to the CT fusion to extract the key characteristics for categorizing the DTI into normal and abnormal cases of MND.

3.3. Proposed DUPLE MONDNet

A Deep MONDNet is proposed for detecting MND at its earliest stages using DTI images from the gathered datasets. CIF and LBP were used for color and texture feature extraction, and Mobile Net was used for classifying normal and abnormal cases of MND.

3.3.1. Color Information Feature (CIF) Block

The CIF block is a specialized component in deep learning models designed for disease detection in medical images, particularly those where color information plays a critical role. This block is engineered to efficiently extract relevant color-related features from the input images, enhancing the model's ability to discriminate between healthy and diseased tissues or structures. By utilizing, the CIF block is designed to capture intricate color patterns and variations within the medical images. It typically consists of a series of convolutional layers, each with learnable filters that convolve over the input image's

color channels (e.g., RGB or other color representations). These filters are designed to detect specific color gradients, textures, or patterns indicative of disease-related characteristics. The output of these convolutional layers is then processed to generate color-related features.

In addition to its convolutional layers, the CIF block may also incorporate advanced techniques like attention mechanisms or feature fusion. These enhancements enable the model to prioritize certain color-related features or integrate them with other relevant information extracted from the image, further improving diagnostic accuracy.

The CIF block stores details about color, including pixel value, contrast, and color dispersion. A color image must initially be divided into many image chunks as the first stage. Figure 2 depicts the RGB conversion in CIF block.

The CIF block is a specialized component in deep learning models that is specifically designed for disease detection in medical images. The CIF block is efficiently extract and process color-related features from the input images. This enhances the model's ability to discriminate between healthy and diseased tissues and thereby improving disease detection. The CIF block captures intricate color patterns and variations within the medical images, which is crucial in identifying disease-related characteristics. An input image undergoes a transformation where its intricate color patterns are extracted and segregated into distinct channels - red, green, and blue. Each channel is then subjected to min and max quantizers identification, that aids in increasing the features essential for accurate disease detection. The CIF block captures intricate color patterns and variations within the medical images. These patterns often correspond to disease-related characteristics. By identifying these patterns, the CIF block detect signs of disease that are missed by other methods. The CIF block is robust to variations in lighting

and color due to its focus on relative color information. This makes it more reliable in different imaging conditions. By prioritizing certain color-related features and integrating them with other relevant information extracted from the image, the CIF block is improving diagnostic accuracy. This is particularly important in medical imaging, where accurate diagnosis can significantly impact patient outcomes. The CIF block processes images in chunks, and it is more computationally efficient. This is crucial in medical imaging, where large volumes of data need to be processed quickly. The CIF block enhances the precision of disease detection in medical images by efficiently extracting and processing color-related features. This not only improves the model's ability to distinguish between healthy and diseased tissues but also captures intricate color patterns and variations within the images, which are often indicative of disease manifestations.

The color reduction method for the color quantizers was carried out after getting the balanced-tree. Each color quantizer, such as the min and max quantizer, receives a single value representation as a result of the color reduction process. Let $T_{min} = \{\widehat{s_1}, \widehat{s_2}, \dots, \hat{s}_{k_{min}}\}$ and $T_{max} = \{\widehat{s_1}, \widehat{s_2}, \dots, \hat{s}_{k_{max}}\}$ be the set of input images from the minimum and maximum quantizer respectively. Here, k_{min} and k_{max} are the dimension of the minimum and maximum color. The $s_{\min}(u, v)$ and $s_{max}(u, v)$ are the minimum and maximum quantizer on image block (u, v). The color extraction method for the minimum quantizer shown in equation (5).

$$\xi\{s_{min}\} = \hat{s}_c \tag{5}$$

Where $c = \{1, 2, \dots, s_{min}\}$ and $\xi\{.\}$ demonstrates the color extracted process of the input images. The color extracted process of the max quantizer is denoted in equation (6).

$$\xi\{s_{max}\} = \hat{s}_d \tag{6}$$

Where $c = \{1, 2, \dots, s_{max}\}$, the above equation demonstrates the nearest pair among the maximum quantizer. The feature extraction phase for the CIF_{min} and CIF_{max} are derived by utilizing equations (7) and (8).

$$CIF_{min}(a) = \chi[\xi(s_{min}(u, v)\} = \hat{s}_c | \mathcal{I} = 1,2, \dots, \tfrac{\mathrm{I}}{\ell}; \mathcal{J} = 1,2, \dots, \tfrac{\mathcal{N}}{\Re}] \quad (7)$$

$$CIF_{max}(a) = \chi[\xi(s_{max}(u, v)\} = \hat{s}_d | \mathcal{J} = 1,2, \dots, \tfrac{\mathrm{I}}{\ell}; \mathcal{J} = 1,2, \dots, \tfrac{\mathcal{N}}{\Re}] \quad (8)$$

The above equation $\chi(.)$ shows the probability factor of min and max quantizer. Here, $c = 1,2, \dots, s_{min}$ and $d = 1,2, \dots, s_{max}$ are identical width of the color extracted feature. The processing of several quantizers, such as the minimum and maximum quantizers from a color image, lead to the creation of a CIF block. It comprises a set of $1x1$ pointwise convolutions (PWConv), a channel shuffling operation, a set of 3x3 depth-wise separable convolutions (DWConv), and finally a channel reordering action. The feature map's result could be demonstrated in a manner is expressed in equation (9).

$$s_f(\mathcal{L}, \Re) = (Q \times N)(\mathcal{L}, \Re) = \sum_a \sum_b Q(a, b)\, Q(\mathcal{L} - a, \Re - b) \quad (9)$$

Where $(\mathcal{L}, \Re)$ shows the input and kernel of the currently accessed phase and s_f represents the characteristic image. The extracted features of CIF block are fused with LBP block for the feature extraction in the classification phase.

3.3.2. Local Binary Pattern (LBP) Block

LBP is a texture descriptor frequently used in conjunction with deep learning techniques for various computer vision tasks. LBP primary role in deep learning is as a feature extraction method. When working with deep neural networks, particularly CNN, LBP is applied as a preprocessing step to capture essential texture information from images. By extracting LBP-based features, the network focus on learning more complex and discriminative features during training.

By extracting LBP features from unlabelled or partially labelled data and using them as input for a deep learning model, it's possible to perform unsupervised or semi-supervised feature learning, which is especially beneficial in medical imaging or other domains with scarce annotated data. LBP plays a valuable part in deep learning by providing a texture-based feature extraction method that enhance the capabilities of deep neural networks in various computer vision applications, especially when data is limited or when capturing local texture information is critical for accurate predictions. The process starts with a grayscale brain scan image. Grayscale images are used to simplify the image while retaining essential information. Color images are converted to grayscale where each pixel corresponds to the intensity of light that it represents. Local Binary Pattern (LBP) is a very efficient texture operator which labels the pixels of an image by thresholding the neighborhood of each pixel and considers the result as a binary number. It’s robust against monotonic gray-scale changes and has shown excellent results in detecting MND. The LBP operation transforms the grayscale image into a texture map. This map emphasizes the different textures present in the image, which correspond to different tissue types in the brain. The texture map makes certain features more distinguishable than the original grayscale image. This method is useful in medical imaging to extract specific features from the images for further analyzing brain diseases. The enhanced contrast image provided by LBP-based feature extraction is aid in identifying areas of interest that might be less noticeable in the original grayscale image.

Diagrammatic representations of the LBP-based feature extraction shown in Figure 3. The textural characteristics of the images are typically captured by image processing systems using an LBP and its variants. For depict retrieval, the visual representation of the LBP pattern serves as an attribute classifier. Before LBP is calculated, a color image

is first converted to grayscale. By evaluating the contents of the central pixel with those of its peers, the LBP generates its code by taking into account the characteristics of the surrounding pixels. The Local Ternary Pattern is a variant of the LBP function, generates three distinct areas in the grey values of the primary pixel and adjacent pixels. The LBP based feature extraction phase of the input image I of size $M \times N$ in RGB color space is initial transformed into the inter-band-average depiction in equation (10),

$$P(x,y) = \frac{1}{3}[R_f(x,y) + G_f(\mathfrak{s},\mathfrak{w}) + B_f(\mathfrak{s},\mathfrak{w})] \quad (10)$$

where $x = 1,2,\dots,M \; and \; y = 1,2,\dots,N$. The factor $(\mathfrak{s},\mathfrak{w})$ represents the pixel location of an image. Although R, G, B, signifies the red, green, blue color space. For the image z_i , the q[th] convolutional layer's characteristic map be illustrated as $conv_i z_i = [conv_i 1\ z_i, conv_i 2\ z_i, \dots, conv_i f\ z_i]$, Where f is the quantity of filters in the q[th] layer of proposed model. For each pixel (u, v) in $conv_i 1\ z_i$, the LBP block is computed in below equation (11).

$$LBP_{s,r}(u,v) = \sum_{\alpha=1}^{s} \varrho(t_v - t_u) \times 2^{n-1} \quad (11)$$

From the above equation, $u \geq 0$; $t_v \; and \; t_u$ $(\alpha = \cdots p)$ denote the intensity values of the pixel (u,v) and p is the neighbour pixel. To express the information about the texture of the image, the occurrences of various binary patterns are gathered into a histogram.

Let $B_{h_{z_i}^{qf}}$ be the texture of histogram extracted feature from $h_{z_i}^{qf}$. For the image z_i, all texture histogram is shown in equation (12)

$$B(z_i) = \{B_{h_{z_i}^1}.B_{h_{z_i}^2}, \dots\dots, B_{h_{z_i}^Q}\} \quad (12)$$

From the above equation $B(z_i)$ be the convolution layer in the fine-tuned model. So $B\left(z_i^{RGB}\right) \; and \; B\left(z_i^{gray\ scale}\right)$ are the color texture histograms from the models. The grey

level value of the pixel (t_v, t_u) in the grey scale factor of the adjacent pixels, where c(x) is denoted in equation (13).

$$s(x) = \begin{cases} 1 \text{ if } x \geq 0 \\ 0 \text{ if } x \geq 0 \end{cases} \quad (13)$$

In deep learning for motor neuron disease classification, the fusion of color and texture features from DTI images be achieved using advanced neural network framework and techniques. The fusion of color and texture features in medical imaging, such as DTI scans, be the valuable approach for motor neuron disease classification. This fusion strategy enhances the sensitivity and specificity of classification models, allowing for more accurate and robust diagnoses of motor neuron diseases. Deep learning techniques, such as Duple-MONDNet, employed effectively to integrate color and texture information from DTI scans and improve the overall performance of disease classification systems. By combining color and texture information in a deep learning model, it becomes more adept at discriminating subtle pathological patterns, leading to more precise and reliable diagnoses of motor neuron diseases from DTI scans.

3.3.3. Mobile Net

Mobile Net is made up of convolutional structures with depth-wise separable convolutions that are more computationally efficient than regular convolutions. The network starts with a series of standard convolutional layers to capture low-level features, followed by depth wise separable convolutions that efficiently extract spatial information while reducing computational load. Depth wise separable convolutions are followed by pointwise convolutions that combine features from different channels. Batch standardization and ReLU layer are applied to enhance network training and stability.

MobileNet typically ends with a global average pooling layer and a fully connected SoftMax layer for categorization.

Following each convolution process, the batch normalization procedure and the ReLU activation feature are employed to achieve automatic data distribution correction. Deep and separable convolution networks speed up Mobile Net training and significantly reduce cost. The standard convolution structure ere denoted in equation (14).

$$\Re_r = \sum_k \omega_{k,l} \cdot \mathrm{I}_k \tag{14}$$

From the above equation $k\ and\ l$ are the input and outcome phase. $\omega_{k,l}$ is the kernel, I_k shows the given data and feature attribute, which utilizing the style of minimum padding. If the dimension of the given input data I_k is $\mathrm{H}_{i_p} \times \mathrm{H}_{i_p}$, the das has l kernel and k channel phase before the feature map access. The computing cost of the standard convolutional layer be shown in equation (15).

$$\mathcal{L}_r = \mathrm{H}_{o/_p} \times \mathrm{H}_{o/_p} \times k \times l \times \mathrm{H}_{i_p} \times \mathrm{H}_{i_p} \tag{15}$$

The depth-wise convolutional phase be demonstrated in equation (16). Where $\wp_{1,k}$ represent the kernels, I_k denotes the input data.

$$\chi_k = \sum \wp_{1,k} \cdot \mathrm{I}_k \tag{16}$$

In depth-wise convolution, k filters with l channels and a $\mathrm{H}_{o/_p} \times \mathrm{H}_{o/_p}$ length is provided. It is important for having l filters during the point-wise iteration with 1×1 dimensions using k channels. The extensive separable convolution structure's computational cost is calculated utilizing equation (17).

$$\mathcal{F}_v = \mathrm{H}_{o/_p} \times \mathrm{H}_{o/_p} \times k \times \mathrm{H}_{i_p} \times \mathrm{H}_{i_p} + k \times l \times \mathrm{H}_{i_p} \times \mathrm{H}_{i_p} \tag{17}$$

Evaluating the above equation of computational cost with the standard convolutional method, the cost of the proposed approach be reduced by $\frac{1}{l} + \frac{1}{\mathrm{H}^2{}_{o/p}}$. Now, the color

extracted features are fed into MobileNet for the classification of MND cases. Architecture of Proposed MobileNet shown in Figure. 4

By using deep and separable convolutional structures, the Mobile Net allows for rapid training and reduced calculations. Finally, the MobileNet is employed for classifying the normal and abnormal cases.

4. Results and Discussion

The MND disease is categorized by utilizing the gathered dataset. The below Figure 5 shows the experimental outcome of the proposed Duple MONDNet model utilizing the gathered dataset. The input images (column 1) are pre-processed using GAB filter (column 2) to reduce the distortion and improve the quality of the input images. Concurrently, these pre-processed images are supplied into color conversion block (column 3) for color feature extraction. The CIF is fuse with LBP block (column 4) for color and texture feature extraction of images in the classification phase. The minimum and maximum value of the RGB conversion images and the extracted features are shown in column (5) & (6), respectively. Finally, the MobileNet is employed for classifying the normal and abnormal cases of MND (column 7).

4.1. Performance Analysis

The results of the investigations demonstrate the specific characteristics, such as precision, sensitivity, specificity, accuracy, recall, and F1 score, of the MND recognition. Basic variables like True Positive ($T_u P_v{}^+$), True Negative ($T_u N_v{}^+$), False Positive ($f_l P_v{}^+$), and False Negative ($f_l N_v{}^+$) is used to provide the discussed evaluation metrics. Accuracy in motor disease classification quantifies the percentage of correctly classified instances, providing a straightforward measure of overall model performance. Using the following equation (18), the accuracy was evaluated.

$$A = \frac{T_u P_v{}^+ + T_u N_v{}^+}{T_u P_v{}^+ + T_u N_v{}^+ + f_l P_v{}^+ + f_l N_v{}^+} \times 100 \quad (18)$$

Precision in deep learning for motor disease classification is a crucial performance metric that measures the accuracy of positive predictions among all predicted positive cases.

$$P = \frac{T_u P_v{}^+}{T_u P_v{}^+ + f_l P_v{}^+} \quad (19)$$

$$Re = \frac{T_u P_v{}^+}{T_u P_v{}^+ + f_l P_v{}^+} \quad (20)$$

$$F1 - Score = \frac{2PreRec}{Pre+Rec} \quad (21)$$

where $T_u P_v{}^+$ and $T_u N_v{}^+$ shows true positives and negatives of input images, $f_l P_v{}^+$ and $f_l N_v{}^+$ depicts the false positives and negatives of the MND images.

The effectiveness of the proposed Duple MONDNet by classifying early stages of MND, including normal and abnormal cases are shown in Table.2. The proposed Duple MONDNet has yield 99.66% accuracy rate. Additionally, the proposed Duple MONDNet achieves an F1 score of 98.44% respectively.

The value for accuracy is displayed on the vertical axis of the Figure 6 reliability curve, while the quantity of phases is plotted on the horizontal axis. The epoch and deficit scale in Figure 7 shows that the data loss of Duple MONDNet minimizes when the epochs are elevated.

The proposed Duple MONDNet classifies early stages of MND using gathered DTI images. To attain the best testing accuracy, this research estimated the number of training epochs sufficient. Depending on the 100 number of epochs, the proposed Duple MONDNet attained 99.66% testing accuracy with a low percentage of errors.

4.2. Comparative analysis

Each neural network's effectiveness was assessed to verify that the Duple MONDNet findings had higher accuracy. Res Net, Alex Net, and Google Net, four neural network classifiers in the proposed Duple MONDNet, were assessed for performance. The quality was estimated by a number of measures, including accuracy, specificity, and recall, which are superior to those employed by conventional DL networks

Table.3 illustrates the contrast by comparing the maximal capacity for categorization over many common DL connections. However, the conventional DL networks failed to produce stronger fallouts than the proposed Duple MONDNet. The proposed Mobile Net raises the overall f1-Score by 2.59%, 3.51%, and 4.14% respectively.

To assess the effectiveness of various strategies, Table 4 provides the experimental result of test images from the gathered dataset. A measure of performance for evaluating prior models was the efficiency of categorization. Comparing the Mobile Net to back-propagation neural network (BPNN), Convolutional Neural Network (CNN), Support vector machine with recursive feature elimination (SVM-RFE), and Multi-Layer Perceptron (MLP) typically results in the f1-score range of 13.26%, 6.15%, 5.56%, and 5.96% respectively.

However, the older networks did not result in superior fallouts than the proposed Duple MONDNet. To distinguish between normal and abnormal cases the indicated Duple MONDNet estimated results seem to be quite reliable.

5. Conclusion

In this research paper, a novel deep learning-based Duple feature extraction for early detection of MND. DTI images are initially analyzed for color and textural features by using dual feature extraction. LBP-based methods extract textural data from an image by examining nearby pixel values. CIF block is then added to the LBP-based feature during

the classification phase for extracting color features. A flattened image is then fed into MobileNet is a classifier that uses the color and texture features of the image to categorize normal and abnormal MND cases. MND cases was detected with an average classification accuracy of 99.66%. A Mobile Net achieves an overall f1-score of 13.26%, 6.15%, 5.56%, and 5.96% over BPNN, CNN, SVM-RFE, and MLP. In the future, the proposed model is extended with advance deep learning techniques, or an advanced color extraction model is implemented for improving the diagnosis rate.

Acknowledgment

The author would like to express his heartfelt gratitude to the supervisor for his guidance and unwavering support during this research for his guidance and support.

References

1. Leigh PN, Ray-Chaudhuri K. Motor neuron disease. Journal of neurology, neurosurgery, and psychiatry 1994; 57 (8): 886. https://doi.org/10.1136/jnnp.57.8.886

2. Tiryaki E, Horak HA. ALS and other motor neuron diseases. CONTINUUM: Lifelong Learning in Neurology 2014; 20 (5): 1185-1207. https://doi.org/10.1212/01.CON.0000455886. 14298.a4

3. Talbot K. Motor neuron disease: the bare essentials. Practical neurology, 2009; 9 (5): 303-309. https://doi.org/10.1136/jnnp.2009.188151

4. Puls I, Jonnakuty C, LaMonte BH, Holzbaur EL, Tokito M et al. Mutant dynactin in motor neuron disease. Nature genetics 2003; 33 (4): 455-456. https://doi.org/10.1038/ng1123

5. Lev S, Halevy DB, Peretti D, Dahan N. The VAP protein family: from cellular functions to motor neuron disease. Trends in cell biology 2008; 18 (6): 282-290. https://doi.org/10.1016/j.tcb.2008.03.006

6. Chiò A, Meineri P, Tribolo A, Schiffer D. Risk factors in motor neuron disease: a case-control study. Neuroepidemiology 1991; 10 (4): 174-184. https://doi.org/10.1159/000110267

7. Sivasankari B, Shunmugathammal M, Appathurai A, Kavitha M. High-Throughput and Power-Efficient Convolutional Neural Network Using One-Pass Processing Elements. Journal of Circuits, Systems and Computers 2022; 31 (13): 2250226. https://doi.org/10.1142/S0218126622502267

8. David AS, Gillham RA. Neuropsychological study of motor neuron disease. Psychosomatics 1986; 27 (6): 441-445. https://doi.org/10.1016/S0033-3182(86)72673-X

9. Sundarasekar R, Appathurai A. Efficient brain tumor detection and classification using magnetic resonance imaging. Biomedical Physics & Engineering Express 2021; 7 (5): 055007. https://doi.org/10.1088/2057-1976/ac0ccc

10. Gallassi R, Montagna P, Morreale A, Lorusso S, Tinuper P et al. Neuropsychological, electroencephalogram and brain computed tomography findings in motor neuron disease. European neurology 1989; 29 (2): 115-120. https://doi.org/10.1159/000116391

11. Drenthen J, Maathuis EM, Visser GH, van Doorn PA, Blok JH et al. Limb motor nerve dysfunction in Miller Fisher syndrome. Journal of the Peripheral Neuron System 2013; 18 (1): 25-29. https://doi.org/10.1111/jns5.12003

12. Gayathri SG, Joseph Jawhar S. A Novel IR Analyzer Based Property Extraction for Segmented Branch Retinal Artery Occlusion and GWO-CNN Based Classification–An Ophthalmic Outcome. IETE Journal of Research 2023; 69 (4): 2164-2176. https://doi.org/10.1080/03772063.2021.1886876

13. Area-Gomez E, Larrea D, Yun T, Xu Y, Hupf J et al. Lipidomics study of plasma from patients suggest that ALS and PLS are part of a continuum of motor neuron

disorders. Scientific reports 2021; 11 (1): 13562. https://doi.org/10.1038/s41598-021-92112-3

14. Carbayo Á, Borrego-Écija S, Turon-Sans J, Cortés-Vicente E, Molina-Porcel L et al. Clinicopathological correlates in the frontotemporal lobar degeneration–motor neuron disease spectrum. *Brain*, awae011. 2024. https://doi.org/10.1093/brain/awae011

15. Kwon HS, Park Y, Kim JH, Kim SH, Jun JB et al. Prevalence of motor neuron diseases in gout patients: a nationwide population-based cohort study. Neurological Sciences 2023; 44 (2): 593-600. https://doi.org/10.1007/s10072-022-06451-8

16. Kanthavel R, Dhaya R, Ahilan A. AI-Based Efficient WUGS Network Channel Modeling and Clustered Cooperative Communication. ACM Transactions on Sensor Networks 2022; 18 (3). https://doi.org/10.1145/3469034

17. Karthikeyan M, Subashini TS, Srinivasan R, Santhanakrishnan C & Ahilan A. YOLOAPPLE: Augment Yolov3 deep learning algorithm for apple fruit quality detection. Signal, Image and Video Processing, 2024; 18(1): 119-128. https://doi.org/10.1007/s11760-023-02710-z

18. Agosta F, Spinelli EG, Riva N, Fontana A, Basaia S et al. Falzone Y, Carrera P, Comi G and Filippi M, Survival prediction models in motor neuron disease. European Journal of Neurology 2019; 26 (9): 1143-1152. https://doi.org/10.1111/ene.13957

19. Lauraitis A, Maskeliūnas R, Damaševičius R, Połap D, Woźniak M. A smartphone application for automated decision support in cognitive task-based evaluation of central neuron system motor disorders. IEEE journal of biomedical and health informatics 2019;23(5):1865-1876. https://doi.org/10.1109/JBHI.2019.2891729

20. Hassanpour A, Moradikia M, Adeli H, Khayami SR, Shamsinejadbabaki P. A novel end-to-end deep learning scheme for classifying multi-class motor imagery

electroencephalography signals. Expert Systems 2019; 36 (6): 12494. https://doi.org/10.1111/exsy.12494

21. Ramakrishnan J, Mavaluru D, Sakthivel RS, Alqahtani AS, Mubarakali A et al. Brain–computer interface for amyotrophic lateral sclerosis patients using deep learning network. Neural Computing and Applications 2020; 1-15. https://doi.org/10.1007/s00521-020-05026-y

22. Zhang K, Xu G, Han Z, Ma K, Zheng X et al. Data augmentation for motor imagery signal classification based on a hybrid neural network. Sensors 2020; 20 (16): 4485. https://doi.org/10.3390/s20164485

23. Greco A, Chiesa MR, Da Prato I, Romanelli AM, Dolciotti C et al. Using blood data for the differential diagnosis and prognosis of motor neuron diseases: a new dataset for machine learning applications. Scientific Reports 2021; 11 (1): 3371. https://doi.org/10.1038/s41598-021-82940-8

24. Subasi A, Mian Qaisar S. The ensemble machine learning-based classification of motor imagery tasks in brain-computer interface. Journal of Healthcare Engineering, 2021. https://doi.org/10.1155/2021/1970769

25. Sekar G, Sivakumar Cmand Logeshwaran J. NMLA: The Smart Detection of Motor Neuron Disease and Analyze the Health Impacts with Neuro Machine Learning Model. Neuro Quantology 2022; 20 (8): 892-899. https://doi.org/10.14704/nq.2022.20.8.NQ44096

26. Bede P, Murad A, Lope J, Shing SLH, Finegan E et al. Phenotypic categorisation of individual subjects with motor neuron disease based on radiological disease burden patterns: A machine-learning approach. Journal of the Neurological Sciences 2022; 432: 120079. https://doi.org/10.1016/j.jns.2021.120079

27. Toh C, Keslake A, Payne T, Onwuegbuzie A, Harding J et al. Analysis of brain and spinal MRI measures in a common domain to investigate directional neurodegeneration in motor neuron disease. Journal of Neurology 2023; 270 (3): 1682-1690. https://doi.org/10.1007/s00415-022-11520-1

28. Sarwinda D, Paradisa RH, Bustamam A, Anggia P. Deep learning in image classification using residual network (ResNet) variants for detection of colorectal cancer. Procedia Computer Science 2021; 179: 423-431. https://doi.org/10.1016/j.procs.2021.01.025

29. Aliyu HA, Razak MAA, Sudirman R, Ramli N. A deep learning AlexNet model for classification of red blood cells in sickle cell anemia. International Journal of Artificial Intelligence 2020; 9 (2): 221-228. https://doi.org/10.11591/ijai.v9.i2.pp221-228

30. Anand R, Shanthi T, Nithish MS, Lakshman S. Face recognition and classification using GoogleNET architecture. In Soft Computing for Problem Solving: SocProS Springer Singapore 2020; 2018 (1): 261-269. https://doi.org/10.1007/978-981-15-0035-0_20

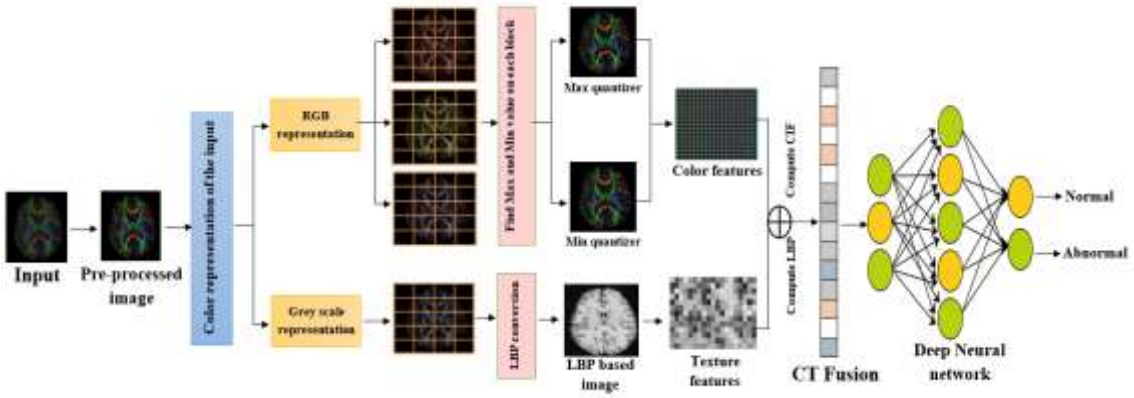

Figure 1 schematic illustration of proposed Duple-MONDNet

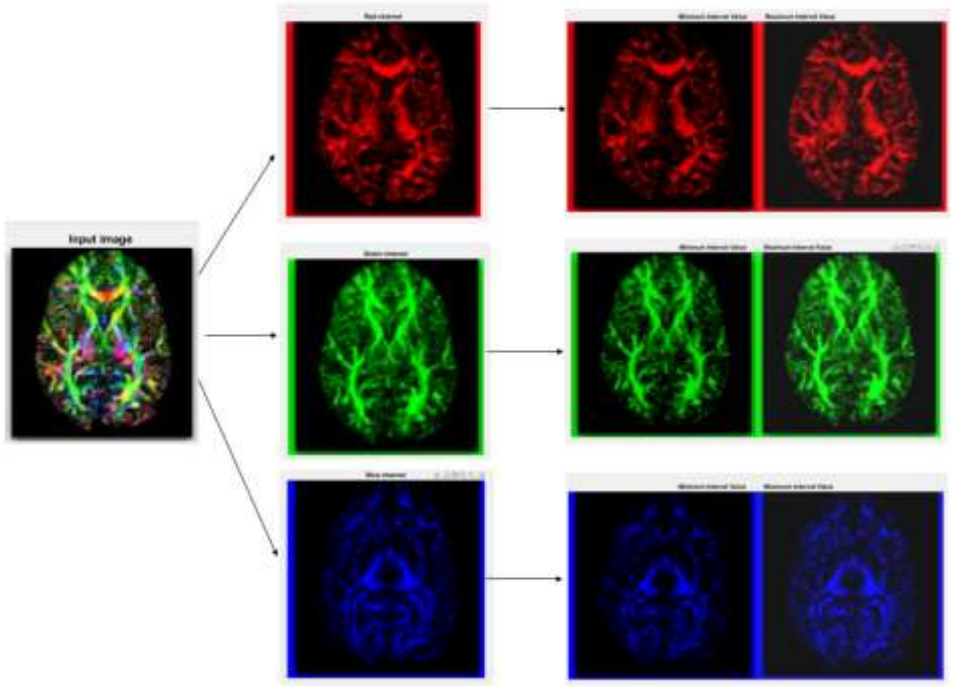

Figure 2 Schematic RGB representation of the min and max quantizers identification

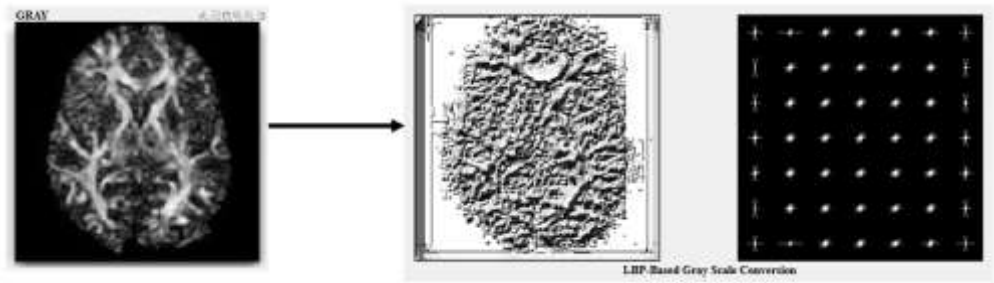

Figure 3 Diagrammatic representations of the LBP-based feature extraction

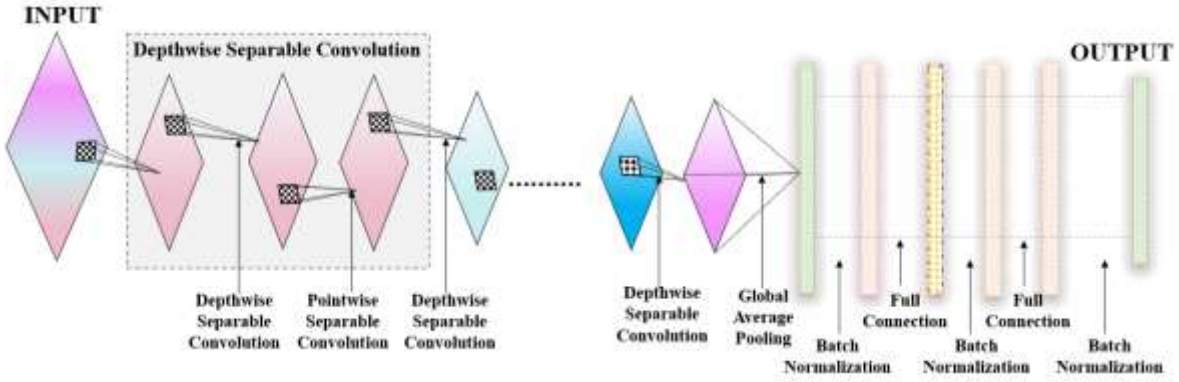

Figure 4 Architecture of Proposed MobileNet

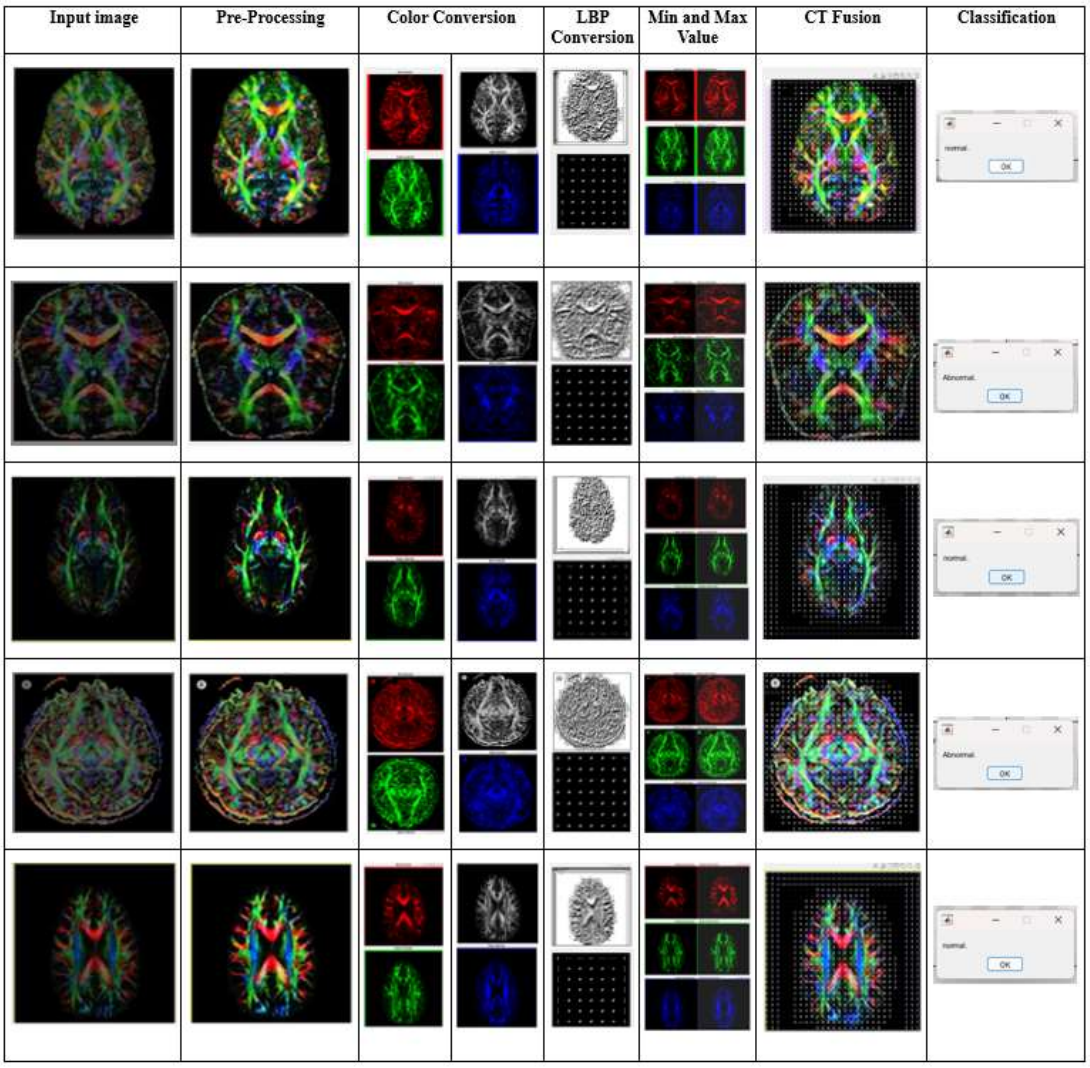

Figure 5. Experimental outcomes of the proposed Duple MONDNet

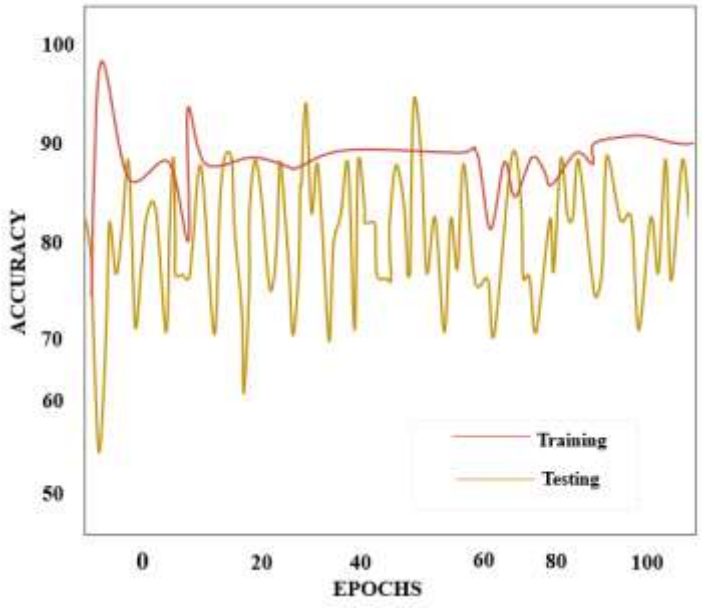

Figure. 6 Accuracy curve of the proposed Duple MOND Net

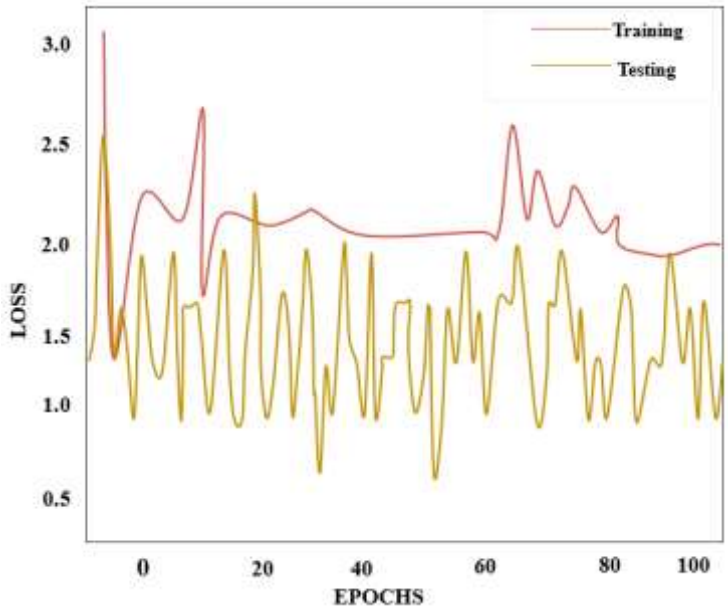

Figure. 7 Loss curve of the proposed Duple MOND Net

Table 1. Dataset description of the proposed model

Disease classes	Before augmentation Self-prepared dataset	After augmentation Self-prepared dataset	Total images
Normal	78	1872	1950
Abnormal	52	1248	1300
Total	130	3120	3250

Table 2. Evaluation outcomes of the proposed Duple MONDNet

Classes	Accuracy	Precision	Recall	Specificity	F1 score
Normal	99.64	98.09	98.33	97.55	98.67
Abnormal	99.68	97.14	97.69	96.66	98.22

Table 3. Comparison with several traditional networks

Networks	Accuracy	Precision	Recall	Specificity	F1 score
Res Net [28]	97.35	97.27	96.36	95.44	97.07
Alex Net [29]	96.17	95.98	97.30	97.453	96.15
Google Net [30]	95.18	94.34	95.63	95.11	95.52
Mobile Net	98.99	98.19	97.21	97.82	98.74

Table4. Accuracy contrast between existing methods and proposed Duple MONDNet

Author	**Methods**	**Accuracy**
Lauraitis, A et al., [19]	BPNN	86.4%
Ramakrishnan, J et al., [21]	CNN	93.51%
Greco, A et al., [23]	SVM-RFE	94%
Bede, P et al., [26]	MLP	93.7%
Proposed model	Duple MONDNet	99.66%